A LINEAR STABILITY ANALYSER SUITABLE FOR INTEGRATION IN WING PERFORMANCE CALCULATION PROCEDURES

Christian Masson* **Marc Langlois†** **Ion Paraschivoiu‡**

Chaire J.-A. Bombardier
École Polytechnique de Montréal
Montréal (Québec), Canada

Abstract

The use of stability analysers based on the linear stability theory and coupled with the e^n method in flowfield calculation procedures (Viscous/Inviscid Interactive methods, Navier-Stokes solvers) has been impeded by the fact that they require tremendous amounts of information, knowledge and interaction from the user. This paper clearly identifies the tasks that demand this interaction and proposes a systematic procedure in order to obtain a linear stability analyser suitable for integration in wing performance calculation procedures. The emphasis is put on the description of a systematic methodology for the location and identification of the instabilities present on a wing. Integration of such a procedure into a linear stability analyser will result in improved efficiency and ease of utilisation. This systematic methodology is based on the matching of tabulated solutions of a model (self-similar) boundary layer with the actual (non-similar) boundary layer growing on a wing. The results obtained so far are very promising. They show that it is possible to represent the stability characteristics of the compressible three-dimensional boundary layer of interest by those of a model boundary layer.

1 Introduction

The ever-present goal of reduced fuel consumption for airliners and business jets has pushed aircraft designers into looking at ways by which skin friction drag can be reduced. A promising avenue lies in maintaining laminar flow over the longest possible portion of the wing, as a turbulent flow produces more friction than a laminar one. Cebeci and his co-workers [1,2] have demonstrated the significant influence a proper prediction of transition can have on the evaluation of the flow characteristics about airfoils at high angles of attack and low Reynolds numbers. It is therefore necessary to be able to predict where the laminar/turbulent transition will take place on a given design, under given flight conditions.

The linear stability theory, coupled with the e^n method, has proven its usefulness in predicting transition, and has been developed to encompass a wide range of flow conditions and geometries. The stability analysers developed until now, though, have mostly been confined to a diagnosis role, to explain the transition behaviour on a configuration and its given flow field, and have yet to be used in flowfield calculation procedures (Viscous/Inviscid Interactive methods, Navier-Stokes solvers). This comes from the the fact that they require tremendous amounts of information, knowledge and interaction from the user. Among the tasks that demand intense interaction are: *(i)* the location and identification of the instabilities present (i.e. where instabilities will appear and what their orientation and wavelength will be), *(ii)* the selection of the critical frequencies that will trigger transition, and *(iii)* the proper tracking of constant-frequency amplification maxima in the integration of the n factor. These problems need to be addressed in a systematic way if an efficient stability analyser, appropriate for incorporation in a global performance calculation procedure, is to be developed. Such is the goal of the research project being currently undertaken.

A systematic procedure for the selection of the critical frequencies has been proposed and described by Masson et al. [3] In this paper, a systematic methodology for the location and identification of the instabilities present on a wing is proposed. This systematic procedure is to be integrated into a linear stability analyser, thus improving its efficiency and making it easier to use.

2 Proposed Methodology

The location and identification of the instabilities present on a wing, i.e. the determination of their inception point, as well as their orientation and wavelength, is conducted with the use of known tabulated solutions of a model (self-similar) boundary layer. Schemes for the rapid evaluation of the stability characteristics of 2-D incompressible flows have been proposed by Stock and Degenhart [4], Dini et al. [5], and Gaster and Jiang [6], amongst others . These methods assume that the velocity profiles on an air-

*Research Scientist, AIAA Member
†Ph.D. Student, AIAA Member
‡Aeronautical Chair Professor, Associate Fellow AIAA

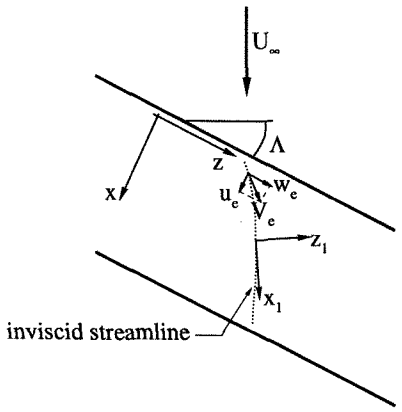

Figure 1: Infinite swept wing flow

foil can be well represented by the Falkner-Skan family of self-similar profiles (the method of Dini et al. also uses modified Green profiles for separated flows). A matching procedure is used to evaluate the stability characteristics of the actual (non-similar) boundary layer profiles of interest from those of the model boundary layer profiles. The calculation of n factors is conducted directly from the model boundary layer stability characteristics. The proposed methodology is an extension of the 2-D incompressible matching method of Gaster and Jiang to 3-D compressible flows, using profiles from a modification of the Falkner-Skan-Cooke family [7]. It is intended to provide a rapid and systematic identification of the instabilities that need to be considered in a "conventional" linear stability analysis, but not to completely replace the stability analysis.

2.1 Model Boundary Layer

To construct the database of stability characteristics, it is necessary to have available a family of boundary layer profiles describing the flow on a three-dimensional wing in compressible flow. For attached, two-dimensional, incompressible flow, the self-similar Falkner-Skan solutions have been used by many authors [4–6]. A similar approach is used in the present work, where a one-species variant of the model proposed by Dewey and Gross [7] has been selected. This model provides a family of compressible boundary layers on an infinite swept wing. Fig. 1 represents the flow under consideration and the coordinate systems used.

The x-momentum, z-momentum and energy equations of the proposed model boundary layer are, respectively:

$$(\lambda f'')' + f f'' = \beta\left(f'^2 - \frac{1}{t_s}\left[(1-t_w)\theta - (1-t_s)g^2 + t_w\right]\right) \quad (1)$$

$$(\lambda g')' + f g' = 0 \quad (2)$$

$$\left(\lambda\frac{\theta'}{\mathrm{Pr}}\right)' + f\theta' = \frac{2\sigma}{1-t_w}\left\{\lambda\left(\frac{1}{\mathrm{Pr}}-1\right)\cdot\left[\left(\frac{u_e}{u_\infty}\right)^2\cos^2\Lambda\, f' f'' + \sin^2\Lambda\, g g'\right]\right\}' \quad (3)$$

The velocity, u, w, and temperature, T, (or enthalpy, H) profiles are defined by

$$f' = f'(\eta) = \frac{u}{u_e} \quad (4)$$

$$g = g(\eta) = \frac{w}{w_e} \quad (5)$$

$$\theta = \theta(\eta) = \frac{H - H_w}{H - H_e} \quad (6)$$

$$H = H(\eta) = c_p T + \frac{u^2 + w^2}{2} \quad (7)$$

and (8)

$$\lambda = \lambda(\eta) = \frac{\rho\mu}{\rho_w\mu_w} = \frac{T_w\mu}{T\mu_w} \quad (9)$$

A prime ($'$) denotes differentiation with respect to η, the normal-to-the-wall coordinate. Subscripts w and e represent quantities at the wall and at the boundary layer edge, respectively, and u_∞ is the component of the freestream velocity U_∞ in the x direction. The independent coordinates (x, y) have been transformed to:

$$\xi(x) = \int_0^x \rho_w\mu_w u_e\, dx \quad (10)$$

$$\eta(x,y) = \frac{u_e}{\sqrt{2\xi}}\int_0^y \rho\, dy \quad (11)$$

The boundary conditions (adiabatic wall) are:

at the wall $f(0) = f'(0) = g(0) = \theta'(0) = 0$ (12)

at the edge $f'(\eta_e) = g(\eta_e) = \theta(\eta_e) = 1$ (13)

The external flow is assumed isentropic, and therefore

$$H_e = \text{constant} = H_0 = c_p T_0 \quad (14)$$

with T_0 the stagnation temperature.

The similarity parameters are

$$\frac{u_e}{u_\infty}, \quad (15)$$

$$\beta = \frac{2\xi}{u_e}\frac{du_e}{d\xi}\frac{T_0}{T_e}t_s, \quad (16)$$

$$\sigma = \frac{U_\infty^2}{2H_e} = \frac{U_\infty^2}{2c_pT_0}, \quad (17)$$

$$t_w = \frac{H_w}{H_e} = \frac{T_w}{T_0} \quad \text{and} \quad (18)$$

$$t_s = 1 - \sigma\sin^2\Lambda \quad (19)$$

It should be noted that for an incompressible flow ($\sigma = 0$) with constant density and viscosity, Eqs. (1) and (2) reduce to the Falkner-Skan-Cooke equations.

Eqs. (1) to (3) are discretised using centred differences on a non-uniform mesh, yielding second-order accuracy for the first derivatives. Starting from initial linear profiles, an iterative procedure is used until the velocity and enthalpy profiles have converged. The non-linear system of equations for f', g and θ is linearised using successive substitution, or Picard, linearisation.

For a prescribed surface temperature (or equivalently a given value of the t_w parameter), this yields tridiagonal systems of equations which can be solved using Thomas algorithm. Since a second-order accurate scheme is used to discretise the adiabatic-wall boundary condition, the tridiagonal structure is lost for the energy system of equations, but can be regained using the Sherman-Morrison formula. A guess of t_w is used to start the calculations. A new value of t_w is calculated after each iteration, from the non-zero value of θ_w and the definition of t_w:

$$t_w^n = t_w^{n-1} + (1 - t_w^{n-1})\theta_w^{n-1} \tag{20}$$

At convergence, $\theta_w = 0$ is obtained.

2.2 Matching Requirements

Physical quantities of interest can be obtained from the above definitions of the five similarity parameters:

$$\mathrm{M}_\infty^2 = \frac{2\sigma}{(\gamma-1)(1-\sigma)} \tag{21}$$

$$\tan^2\Lambda = \frac{1-t_s}{\sigma+t_s-1} \tag{22}$$

$$u_e^2 = 2\,c_p T_0\,(\sigma+t_s-1)\left(\frac{u_e}{u_\infty}\right)^2 \tag{23}$$

$$w_e^2 = 2\,c_p T_0\,(1-t_s) \tag{24}$$

$$T_e = T_0\left(t_s - (\sigma+t_s-1)\left(\frac{u_e}{u_\infty}\right)^2\right) \tag{25}$$

$$\mathrm{M}_\mathrm{e}^2 = \frac{2}{\gamma-1}\frac{1-t_s+(\sigma+t_s-1)\left(\frac{u_e}{u_\infty}\right)^2}{t_s-(\sigma+t_s-1)\left(\frac{u_e}{u_\infty}\right)^2} \tag{26}$$

where M_∞ and M_e are the Mach numbers related to U_∞ and V_e ($= \sqrt{u_e^2+w_e^2}$), respectively.

For the matching with the actual boundary layer growing on a wing and the calculation of the stability characteristics, it is useful to define a coordinate system that is aligned with the streamline at the edge of the boundary layer (x_1, z_1 system in Fig. 1). The velocity profiles in this system are:

$$\frac{u_1}{V_e} = \frac{u_e^2 f' + w_e^2 g}{u_e^2+w_e^2} \tag{27}$$

$$\frac{w_1}{V_e} = \frac{u_e w_e}{u_e^2+w_e^2}(g-f') \tag{28}$$

The matching procedure uses the incompressible shape factors in the streamwise and crossflow directions, defined as:

$$h_{x_i} = \frac{\delta_{x_i}}{\theta_{x_i}} \tag{29}$$

$$h_{z_i} = \frac{\delta_{z_i}}{\theta_{z_i}} \tag{30}$$

where

$$\delta_{x_i} = \int_0^\infty \left(1-\frac{u_1}{V_e}\right)d\eta \tag{31}$$

$$\delta_{z_i} = \int_0^\infty -\frac{w_1}{V_e}d\eta \tag{32}$$

$$\theta_{x_i} = \int_0^\infty \frac{u_1}{V_e}\left(1-\frac{u_1}{V_e}\right)d\eta \tag{33}$$

$$\theta_{z_i} = \int_0^\infty -\left(\frac{w_1}{V_e}\right)^2 d\eta \tag{34}$$

As mentionned earlier, there are five non-dimensional parameters that specify a given self-similar boundary layer: σ, t_s, t_w, β and u_e/u_∞. The aim of the matching procedure is to determine the combination of these parameters that will produce a model boundary layer having stability characteristics similar to those of the actual boundary layer of interest. In this work only adiabatic-wall boundary layers are considered. In this case, there is only one possible value of t_w for a given combination of the other parameters. The σ and u_e/u_∞ parameters can be obtained directly from the flow conditions of the physical boundary layer, by inverting Eqs. (21) and (26):

$$\sigma = \frac{\frac{\gamma-1}{2}\mathrm{M}_\infty^2}{1+\frac{\gamma-1}{2}\mathrm{M}_\infty^2} \tag{35}$$

$$\left(\frac{u_e}{u_\infty}\right)^2 = \frac{\left(1+\frac{\gamma-1}{2}\mathrm{M}_\mathrm{e}^2\right)t_s - 1}{(\sigma+t_s-1)\left(1+\frac{\gamma-1}{2}\mathrm{M}_\mathrm{e}^2\right)} \tag{36}$$

For the determination of the remaining two parameters (t_s and β) it is necessary to require that some "measurable" properties of the model boundary layer be as close as possible to the same properties measured on the actual boundary layer on the wing. Following the approach taken in two-dimensional incompressible flows, the incompressible shape factor in the local streamwise direction (h_{x_i}), is matched. This should ensure closeness of the streamwise velocity profiles (u_1/V_e). By extension, the second property may be chosen to be the incompressible shape factor in the crossflow direction (h_{z_i}). This is one of the options considered in this work. The possibility of using the maximum crossflow velocity and the non-dimensional crossflow-velocity derivative at the wall as matching

properties is also considered here. The latter quantities are defined as:

$$w_{1_{max}} = \max_{\eta} \left| \frac{w_1}{V_e} \right| \quad (37)$$

$$w'_{1_w} = \frac{\delta_{x_i}}{V_e} \frac{dw_1}{d\eta} \bigg|_w \quad (38)$$

2.3 Linear Stability Theory

The basis of the linear stability theory is the decomposition of the instantaneous flow variables into a mean, steady part and a time-dependent perturbation of a sinusoidal form:

$$q(x,y,z,t) = Q(y) + \tilde{q}(y) e^{i(\alpha x + \beta z - \omega t)} \quad (39)$$

where q represents any of the flow variables (i.e. the velocity components u_1, v, w_1 in the streamwise (x_1), wall-normal (y) and crossflow (z_1) directions, the pressure p and the temperature T). $Q(y)$ represents the laminar mean flow, which is assumed to be parallel, while α and β are the streamwise and crossflow wave numbers of the perturbation and ω its complex frequency.

After substitution of Eq. (39) into the governing equations, subtraction of the laminar mean flow solution and linearisation, a homogeneous system of five second-order ordinary differential equations is obtained. Given homogeneous boundary conditions, the task then reduces to the resolution of an eigenvalue problem for the determination of the values of the complex parameters α, β and ω that yield non-trivial solutions.

The eigenvalue problem provides two real relations, but there are six real parameters to be determined. Basic assumptions about the nature of the eigenvalues are therefore required. It is customary to specify that one or two of the parameters be pure real numbers. In the case of the temporal stability theory used in the present work, α and β are assumed to be real. One can see then that the real part of ω, ω_r, corresponds to the frequency and its imaginary part, ω_i, to the temporal growth rate of the perturbation.

Since the eigenvector, $\tilde{q}$, depends only on y and the mean flow has been assumed parallel, it is possible to apply a local analysis, i.e. the determination of the stability characteristics at a given point on a wing involves only the local boundary layer properties, no information is required from the neighbourhood. This is the essential feature that allows pre-calculated stability characteristics of model boundary layers to be used for the identification and location of the instabilities in the actual boundary layer growing on a wing.

3 Results

To demonstrate the capacity of the model boundary layers presented in Section 2.1 to adequately estimate the stability characteristics of the actual boundary layer growing on a wing, three test cases are considered. Comparisons between the stability characteristics calculated with the actual boundary layer profiles and those obtained with the model boundary layer profiles selected with various matching parameters are presented. The actual boundary layer profiles on a wing were calculated using the characteristics method of Houdeville et al. [8] In the discussion of the results that follows, these boundary layers and their properties are referred to as "exact". It is important to note that the stability characteristics presented in the paper have been normalized with V_e as the reference velocity and δ_{x_i} as the length scale.

	Inf. SW #2	matching		
		$w_{1_{max}}$	h_{z_i}	w'_{1_w}
$\Lambda(°)$	25	49	49	39
t_s	—	0.927	0.927	0.978
β	—	0.310	0.310	0.310
h_{x_i}	0.415	0.415	0.415	0.420
h_{z_i}	-0.044	-0.044	-0.044	-0.035
$w_{1_{max}}$	-0.060	-0.060	-0.060	-0.045
w'_{1_w}	-0.102	-0.131	-0.131	-0.102
$\frac{T_w}{T_e}$	1.188	1.190	1.190	1.190

Table 1: Matching parameters — Inf. SW #2

3.1 Infinite swept wing

The first test case concerns an infinite wing with a sweep angle of 25° and a supercritical profile. This is the wing referred to as Wing #2 in Ref. (3). The flow conditions under study are: $M_\infty = 0.855$, $C_L = 0.40$ and $Re = 11.0 \cdot 10^6$. Fig. 2 shows the exact boundary layer profiles on the wing at $x/c \simeq 0.2$, in a region of strong favourable pressure gradient. Also shown are the model boundary layer profiles that were obtained by matching h_{x_i} and one of the following quantities: h_{z_i}, $w_{1_{max}}$ or w'_w. The values of these matching parameters are summarized in Table 1.

To verify the pertinence of using Eq. (36) to determine the parameter u_e/u_∞ directly from the exact local Mach number, M_e, model boundary layers were calculated for a range of values of u_e/u_∞. It was found that the solution that matched the exact T_w was indeed the one for which M_e was matched.

The matching is excellent for the streamwise velocity and temperature profiles, but more significant differences are observed in the crossflow velocity profile, related mainly to the height at which the maximum velocity occurs. This distance seems to be independent of the matching parameter used. Tests have indicated that it depends mostly on β, which is closely related to the streamwise shape factor h_{x_i}. It is also im-

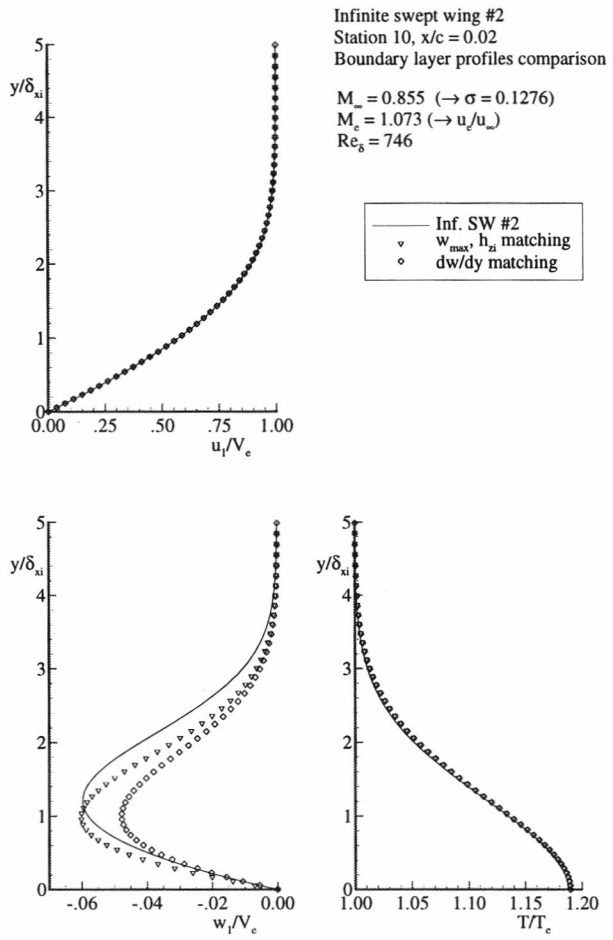

Figure 2: Boundary layer profiles — Inf. SW #2

portant to notice that the sweep angles for the model boundary layers (49° and 39°, see Table 1) are not equal to the actual infinite wing sweep angle (25°).

The stability characteristics calculated with the exact boundary layer are displayed in Fig. 3. In this figure, as in all other stability diagrams presented, the shades of grey represent the amplification rate (ω_i) of the instability , while the value-labelled lines represent its frequency (ω_r). As expected for a boundary layer without a streamwise inflection point, there is only one significant amplification maximum, corresponding to a crossflow instability. Fig. 4 presents the stability characteristics for the model boundary layers of Fig. 2.

The overall agreement between the exact and model stability characteristics is quite good. The position (wave number and orientation) of the maximum crossflow instability is well reproduced by the model bounday layers, albeit with lower amplification rates, especially for the w'_{1_w} matching. This was to be expected, since the latter model solution has a smaller maximum crossflow velocity than the exact boundary layer.

As the proposed model boundary layer is also to be

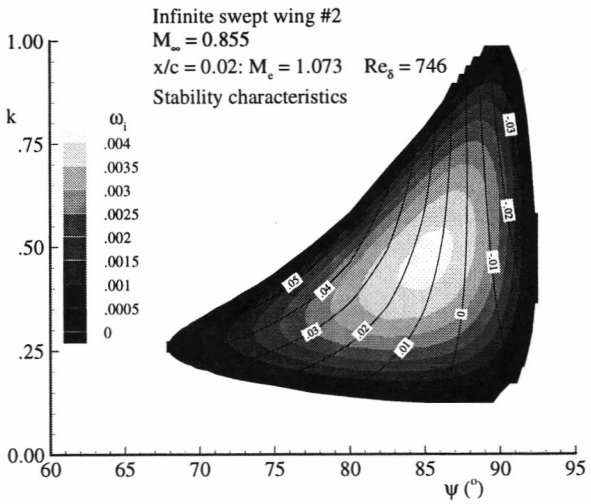

Figure 3: Stability characteristics — Inf. SW #2

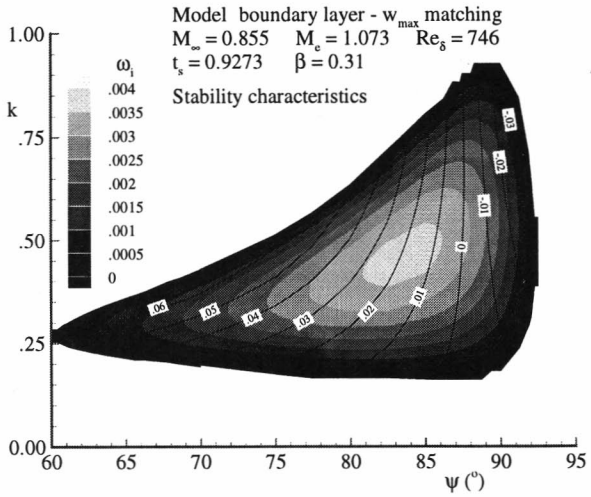

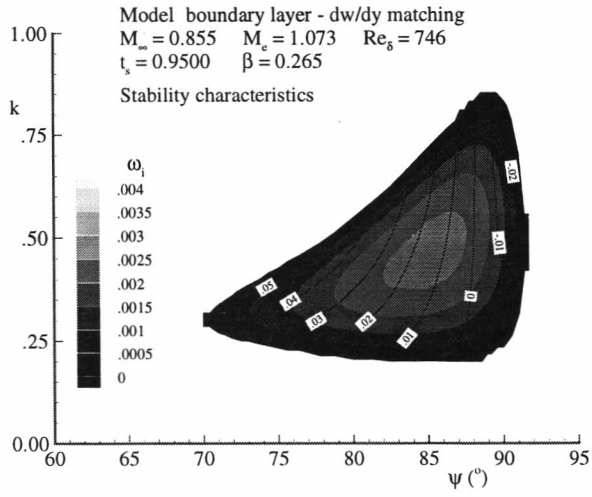

Figure 4: Stability characteristics — Model BL (1)

used to identify the instabilities that are relevant in the estimation of transition, i.e. the calculation of n factors, it should provide a good representation of the maximum amplification, and its associated wave orientation and wave number (wave vector), as a function of frequency ($\omega_{i_{max}}$, ψ and k vs. ω_r). Fig. 5 presents this evolution and the associated wave numbers and wave orientations for the exact and model boundary layers. The model boundary layer with $w_{1_{max}}$ matching shows less amplification than the exact solution for frequencies below 0.03. Its maximum amplification rate is $\omega_{i_{max}} = 0.0037$ at a frequency of 0.02. This compares with a maximum amplification of 0.0042 at $\omega_r = 0.015$ for the exact boundary layer. Above $\omega_r = 0.03$, the amplification rate of the model boundary layer becomes increasingly larger than that of the exact one. Neutral amplification is reached at $\omega_r \simeq 0.073$ in the model boundary layer calculations, compared to approximately 0.059 in the exact ones. The amplification levels of the w'_{1_w}-matched model boundary layer are significantly lower than the exact ones over the whole range of unstable frequencies ($\omega_{i_{max}} = 0.0022$ at $\omega_r = 0.02$, neutral amplification at $\omega_r = 0.055$). The bottom part of Fig. 5 shows that the orientation of the most unstable wave is well represented by both model boundary layer solutions, and so is the wave number.

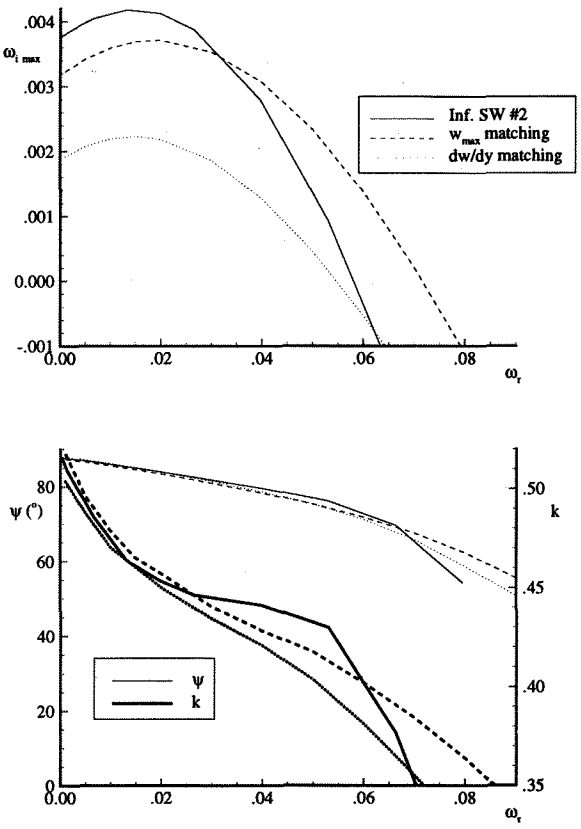

Figure 5: Evolution of $\omega_{i_{max}}$ — Inf. SW #2

3.2 NASA AMES wing

For the second test case, we investigated the stability of the boundary layer in a region of mild adverse pressure gradient on the NASA AMES swept wing [9]. The flow conditions for this case are: $M_\infty = 0.833$, $\alpha = 1.75°$ and $Re = 14.3 \cdot 10^6$. More details about the wing geometry and detailed stability calculations can be found in Ref. (9). Fig. 6 shows the exact boundary layer profiles on the wing, compared with the model boundary layer profiles obtained with the three matching methods. The matching parameters are presented in Table 2. Once again, the inflected streamwise velocity profile and the temperature profile are in near-perfect agreement, but differences are significant in the crossflow velocity distribution. The wall-derivative matching produces a maximum crossflow velocity that is only one-fourth of the exact one. The shape factor and maximum velocity matchings produce nearly the same result, but with a maximum that is significantly closer to the wall. It should be noted that the exact boundary layer profile exhibits two points of inflection, but all the model boundary layer solutions have only one point of inflection.

We next present on Figs. 7 and 8 the stability diagrams obtained with the exact boundary layer and the $w_{1_{max}}$- and w'_{1_w}-matched model boundary layers. The results for the h_{z_i} matching should be very similar to those of the maximum velocity matching. Fig. 7 shows that three local maxima of amplification are present, which is typical of a region of mild adverse pressure gradient. The highest levels of amplification are encountered in the region around $\psi = -50°$, but it is expected that the most significant region of the diagram, for transition prediction, is that around $\psi = 50°$. This assertion is justified by the fact that instability amplification on a wing usually starts near the leading edge with crossflow waves (at $\psi \simeq 90°$). As waves travel downstream and the crossflow instability attenuates, it seems logical to track the evolution of the streamwise maximum that is closer in orientation. The model solutions show only two instability maxima, the crossflow local maximum being absent.

Fig. 9 shows the evolution of the maximum amplification rate and the associated wave number and orientation as a function of frequency. Only the crossflow (label (1)) and positive streamwise (label (2)) instabilities have been considered. For frequencies below 0.025, the maximum amplification of the exact boundary layer belongs to a crossflow wave. The bottom part of Fig. 8 shows that at low frequencies, the most unstable direction for the model boundary layer solutions goes towards 90°, but this is related to the streamwise local maxima, and the equivalent of branch (1) of the exact solution is absent from the

	NASA AMES	matching		
		$w_{1_{max}}$	h_{z_i}	w'_{1_w}
t_s	—	0.940	0.944	0.996
β	—	-0.057	-0.057	-0.057
h_{x_i}	0.376	0.376	0.376	0.374
h_{z_i}	-0.011	-0.012	-0.011	-0.003
$w_{1_{max}}$	-0.016	-0.016	-0.015	-0.004
w'_{1_w}	-0.010	-0.036	-0.035	-0.010
$\frac{T_w}{T_e}$	1.286	1.287	1.287	1.287

Table 2: Matching parameters — NASA AMES wing

model boundary layer solutions. The maximum amplification occurs at $\omega_r \simeq 0.05$ for the exact and both model boundary layers. The value of this maximum is overpredicted by about 20% by the $w_{1_{max}}$-matched model boundary layer and by about 6% by the w'_{1_w}-matched one. The amplification levels predicted by the $w_{1_{max}}$-matched model boundary layer are larger than the exact ones over the whole range of unstable frequencies, while the w'_{1_w}-matched solution shows a better overall agreement. These differences can be attributed to the value and distance from the surface of the maximum crossflow velocity. The lower part of the figure also shows that the wave orientation and direction are in slightly better agreement with the exact solution (branch (2)) for the wall derivative matching than for the maximum velocity matching.

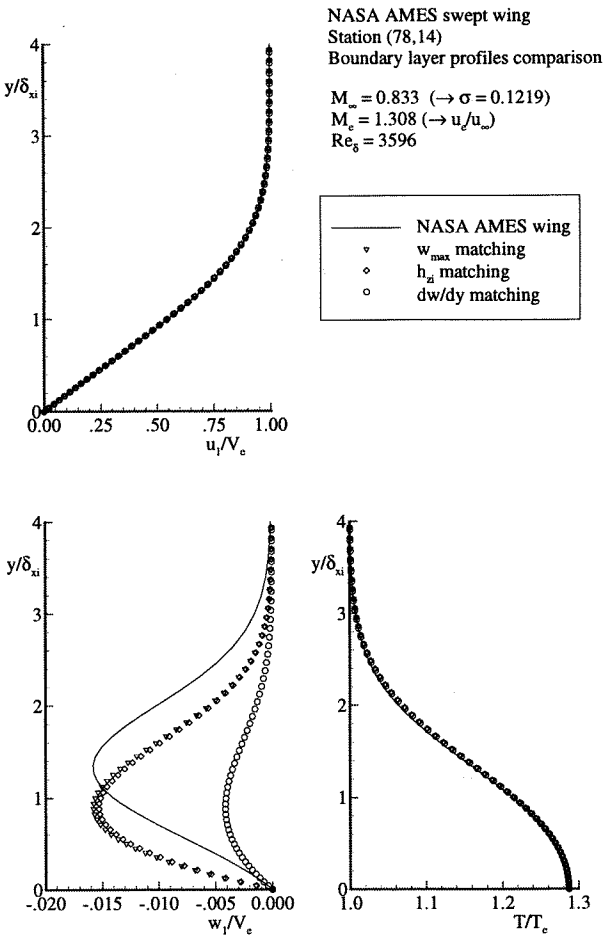

Figure 6: Boundary layer profiles — NASA wing

3.3 ONERA M6 wing

The final test case concerns a boundary layer in a strong adverse pressure gradient on the ONERA M6 wing. The flow conditions in this case are: $M_\infty = 0.84$, $\alpha = 3.06°$, $Re = 11.7 \cdot 10^6$. The results of detailed calculations were published in Refs. (9,10). The boundary layer profiles corresponding to the matching parameters given in Table 3 are compared to the exact solution on Fig. 10. The crossflow velocity profile exhibits two maxima (in absolute value), and it is obvious that none of the model boundary layer solutions comes close to representing it. It should be noted that the $w_{1_{max}}$ matching was applied to both maxima, denoted by the subscripts "low" and "up" in the figures. It can be observed that the distance of the crossflow maximum from the surface is the same for all the model boundary layer profiles, resulting in a positive maximum that is further from the surface ($w_{1_{max,low}}$ and w'_{1_w} matchings) or a negative maximum that is closer to the surface ($w_{1_{max,up}}$ and h_{z_i} matchings).

Fig. 11 shows the stability characteristics calculated with the exact boundary layer profiles. Three local maxima can be observed. The most important one is at $\psi \simeq -60°$, but it is expected that the instabilities with a positive ψ will play a more important role in transition, for the same reason as given in the previous section. The stability diagrams obtained by matching both crossflow velocity maxima and the crossflow velocity wall derivative are presented on Fig. 12. The pure crossflow local maximum is absent from all model boundary layer calculations. The wave number and orientation at which the two streamwise maxima occur are well reproduced. The better overall agreement with the exact solution seems to be obtained in this case for the model boundary layer with w'_{1_w} matching. This is confirmed by Fig. 13, where label (1) refers to crossflow instabilities and label (2) refers to streamwise instabilities (of the exact boundary layer solution, Fig. 11). The model boundary layers obtained by matching $w_{1_{max,low}}$ and w'_{1_w} provide levels of amplification that are very close to the streamwise branch (2) of the exact boundary layer solution, with the w'_{1_w}-matched results being slightly closer up to $\omega_r \simeq 0.18$. The $w_{1_{max,up}}$-matched model boundary layer produces levels of amplification that are up to 70% higher than those of the exact boundary layer. This is explained by the fact that the maximum crossflow velocity for

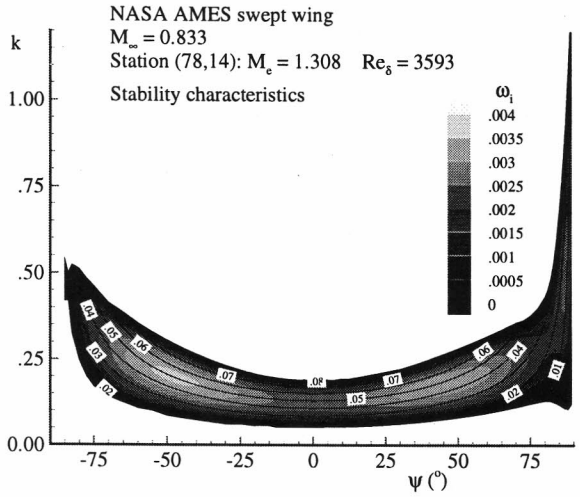

Figure 7: Stability characteristics — NASA wing

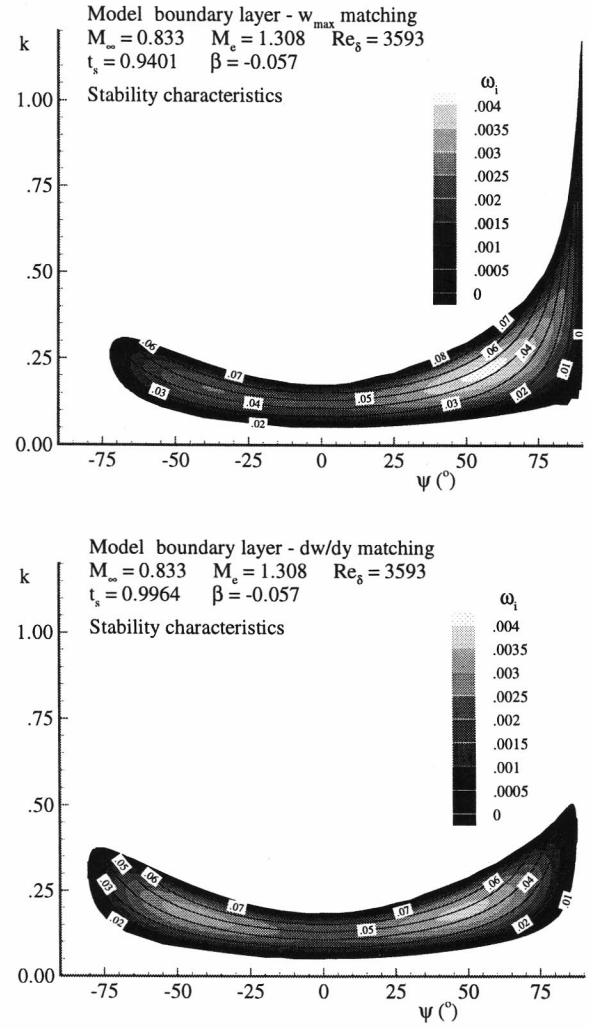

Figure 8: Stability characteristics — Model BL (2)

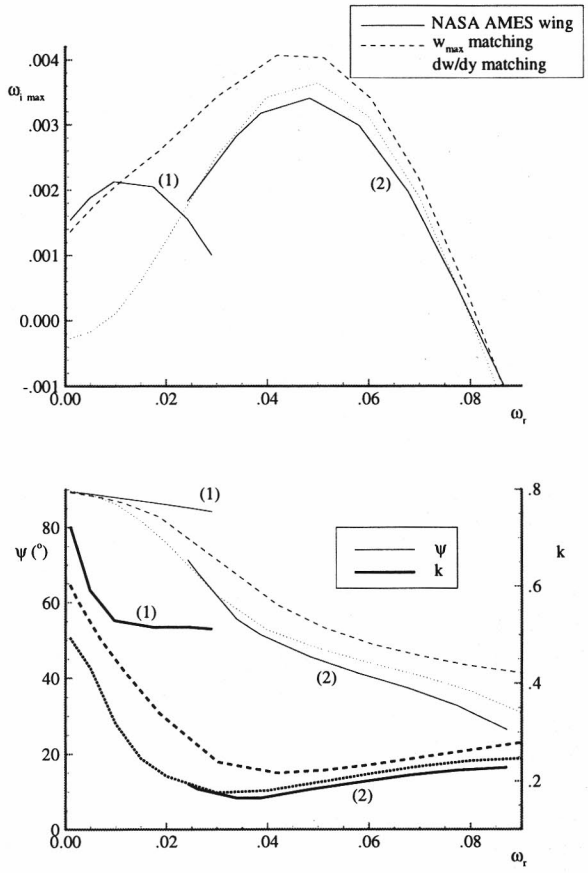

Figure 9: Evolution of $\omega_{i_{max}}$ — NASA AMES wing

this boundary layer occurs much closer to the surface than the negative maximum of the exact boundary layer.

3.4 Summary of Results

The model boundary layers are defined by five similarity parameters: t_w, σ, u_e/u_∞, β and t_s. The adiabatic-wall boundary condition determines the first of these (t_w), as a function of the other four. The freestream Mach number (M_∞) and the Mach number at the edge of the (exact) boundary layer (M_e) directly provide two more parameters (σ and u_e/u_∞). The last two parameters are related to the local sweep angle and pressure gradient and have to be identified by matching some global properties of the velocity profiles. The streamwise incompressible shape factor (h_{x_i}) has been found to provide a very good representation of the streamwise velocity profile, even in strongly decelerated flows. It has also been observed that the value of the pressure-gradient parameter (β) is almost uniquely determined by this shape factor. The matching of the crossflow velocity profile is less straightforward. The distance of the crossflow velocity maximum from the surface and the presence of multiple crossflow velocity maxima are features

	ONERA M6	matching			
		$w_{1_{mx,l}}$	$w_{1_{mx,u}}$	h_{z_i}	w'_{1_w}
t_s	—	0.997	0.993	0.975	0.986
β	—	-0.180	-0.180	-0.180	-0.180
h_{x_i}	0.315	0.314	0.314	0.316	0.315
h_{z_i}	-0.036	0.012	-0.018	-0.036	0.027
$w_{1_{max}}$	0.017	0.017			0.036
	-0.024		-0.025	-0.048	
w'_{1_w}	0.094	0.044	-0.064	-0.125	0.095
$\frac{T_w}{T_e}$	1.348	1.361	1.361	1.360	1.360

Table 3: Matching parameters — M6 wing

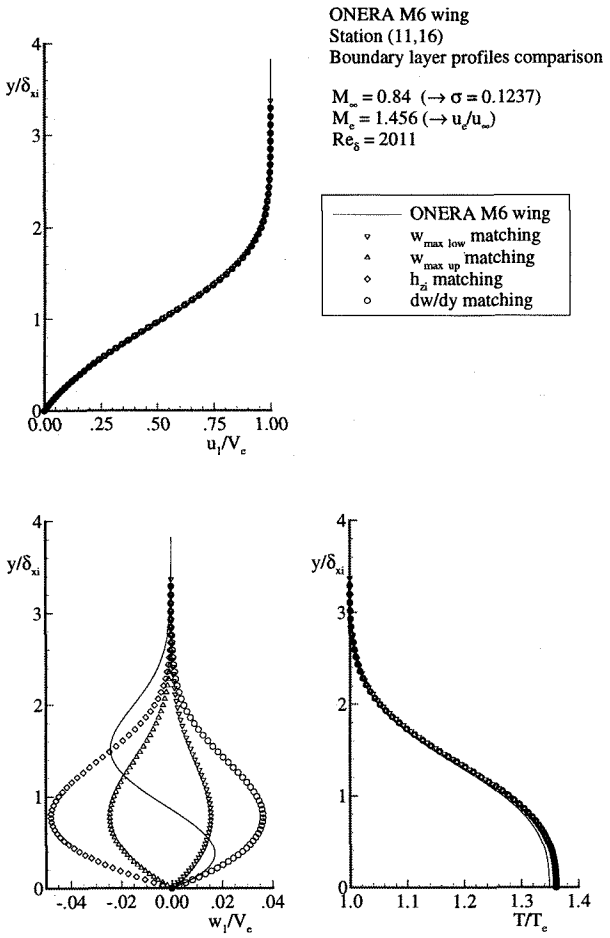

Figure 10: Boundary layer profiles — M6 wing

that have a strong influence on the stability characteristics. Three different crossflow matching parameters have been tested: the crossflow incompressible shape factor (h_{z_i}), the maximum crossflow velocity ($w_{1_{max}}$) and the crossflow velocity derivative at the wall (w'_{1_w}). In accelerated flows ($\beta > 0$), where the importance of the crossflow velocity profile is greatest, the $w_{1_{max}}$-criterion seems to produce the best agreement of velocity profiles and stability characteristics, with the h_{z_i}-criterion being almost equally good. It should be pointed out, though, that only one test case has been conducted for favourable pressure gradient. Two test cases have been studied for decelerated flows ($\beta < 0$), where streamwise instabilities become dominant. These tend to show that the w'_{1_w} matching provides a better representation of the streamwise instabilities than the other matching criteria, even though the resulting model boundary layer may show a crossflow velocity maximum that is many times greater or smaller than that of the exact boundary layer.

4 Conclusions

The essential features of a linear stability analyser suitable for integration in wing performance calculation procedures have been identified. One of these features is the systematic location and identification of the instabilities present on a wing. A procedure capable of achieving this task has been proposed in this paper. This procedure is based on the use of pre-calculated stability characteristics for a family of model boundary layers to represent the stability characteristics of the actual boundary layer growing on a wing. The three-dimensional compressible model boundary layers are defined by five similarity parameters.

The results obtained so far look very promising. They show that it is possible to represent the stability characteristics of the compressible boundary layer growing on an arbitrary three-dimensional wing by those of a model boundary layer. More tests will be required in order to identify the best matching procedure for the crossflow velocity profile, keeping in mind that what must ultimately be reproduced is not so much the velocity profile itself but the boundary layer stability characteristics. A criterion that integrates two or more of the parameters used so far, such as that proposed by Stock and Degenhart [4] for incompressible 2-D flow, might be useful. The model boundary layer used in this work is valid only for attached boundary layer flow. The possibility of using a 3-D compressible extension of the modified Green family of profiles [5] to represent separated boundary layers will also be investigated.

Acknowledgements

This work was supported in part by the Natural Sciences and Engineering Research Council of Canada, through a R & D Grant, in collaboration with Bombardier Inc./Canadair. The second author would also like to acknowledge the assistance provided by the Fonds pour la Formation de Chercheurs et l'Aide à la Recherche (Gov. of Québec) in the form of a post-

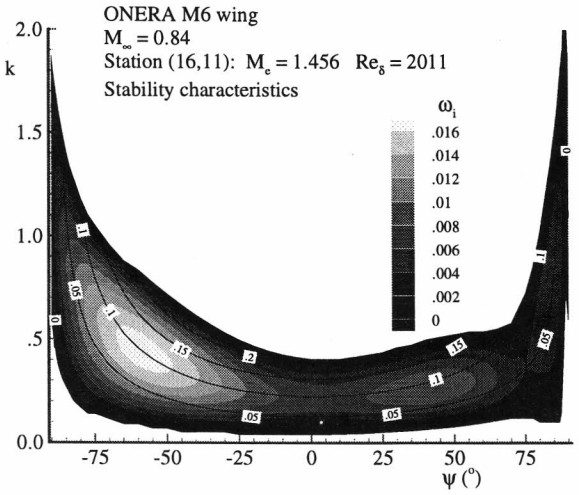

Figure 11: Stability characteristics — M6 wing

graduate scholarship, and the Advanced Aerodynamics Department at Canadair, where most of the calculations presented were performed.

References

(1) Cebeci, T., Clark, R.W., Chang, K.C., Halsey, N.D. and Lee, K. "Airfoils with Separation and the Resulting Wakes". *Journal of Fluid Mechanics*, **153:** 323-347 (1986).

(2) Cebeci, T. "Essential Ingredients of a Method for Low Reynolds-Number Airfoils". *AIAA Journal*, **27, no. 12:** 1680-1688 (1989).

(3) Masson, C., Martinuzzi, R., Langlois, M., Paraschivoiu, I. and Tezok, F. "Transition Prediction Capabilities for Conical Wings in the Transonic Regime". *Canadian Aeronautics and Space Journal*, **41:** 28-39 (1995).

(4) Stock, H.W. and Degenhart, E. "A simplified e^n method for transition prediction in two-dimensional, incompressible boundary layers". *Z. Flugwiss. Weltraumforsch.*, **13:** 16-30 (1989).

(5) Dini, P., Selig, M.S. and Maughmer, M.D. "Simplified Linear Stability Transition Prediction Method for Separated Boundary Layers". *AIAA Journal*, **30, no.8:** 1953-1961 (1992).

(6) Gaster, M. and Jiang, F. "A Rapid Scheme for Estimating Transition on Wings by Linear Stability Theory". *ICAS Paper 94-2.4.3, Proceedings of the 19th Congress of the International Council of the Aeronautical Congress*, **3:** 1104-1113, Anaheim (1994).

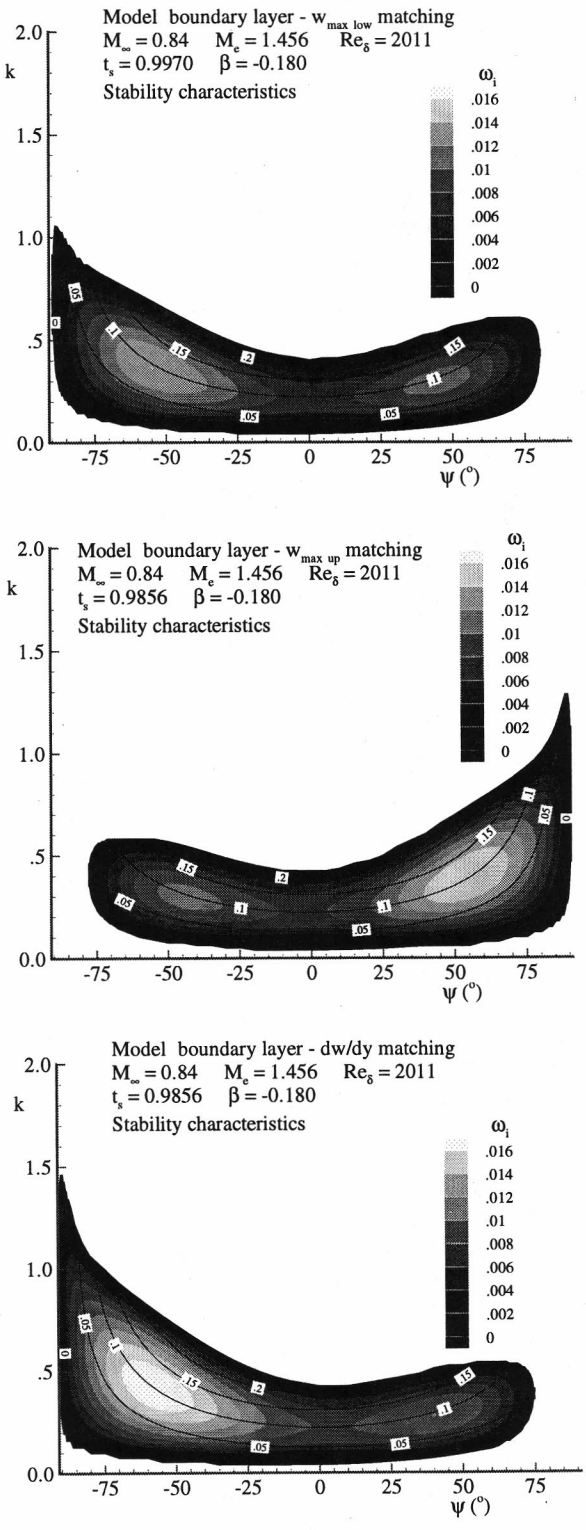

Figure 12: Stability characteristics — Model BL (3)

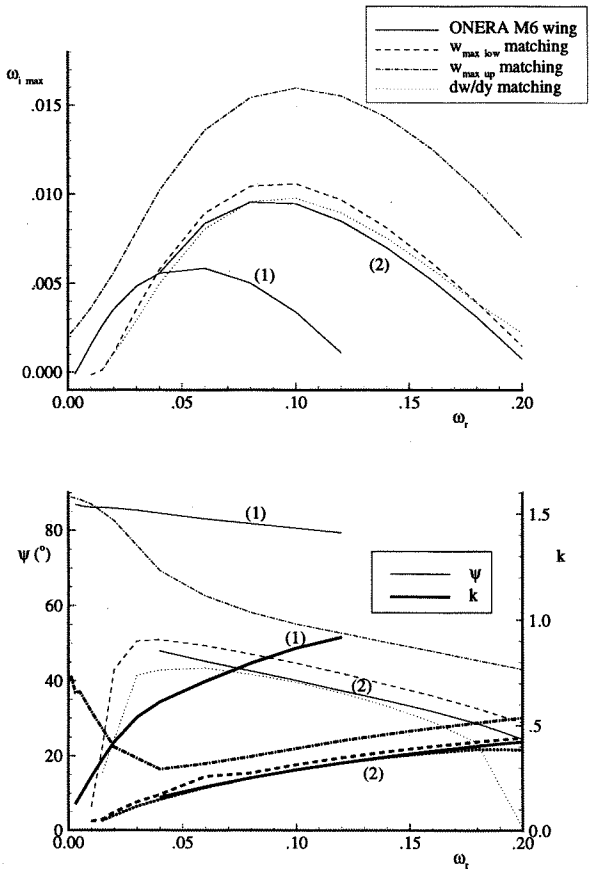

Figure 13: Evolution of $\omega_{i_{max}}$ — ONERA M6 wing

(7) Dewey, C.F. and Gross, J.F. "Exact Similar Solutions of the Laminar Boundary Layer Equations". *Advances in Heat Transfer*, **4:** 317-446 (1967).

(8) Houdeville, R., Mazin, C. and Corjon, A. "Méthode de caractéristiques pour le calcul des couches limites tridimensionnelles". *La Recherche Aérospatiale*, **1:** 37-49 (1993).

(9) Langlois, M., Masson, C. and Paraschivoiu, I. "Transition Prediction in Three-Dimensional Transonic Flows". *Numerical Methods in Laminar and Turbulent Flow (Proceedings of the Ninth International Conference)*, **9 (Part 1):** 493-504, Atlanta (1995).

(10) Masson, C., Langlois, M. and Paraschivoiu, I. "Analysis of the Transition Characteristics of Three-Dimensional Transonic Flows". *Proceedings of the Second Annual Conference of the CDF Society of Canada (CFD94)*, 535-542, Toronto (1994).